Supplementary Information

Direct imaging of nanoscale field-driven domain wall oscillations in Landau structures

Balram Singh,[a,b] Rachappa Ravishankar,[a] Jorge. A. Otálora,[c] Ivan Soldatov,[a] Rudolf Schäfer,[a,d] Daniil Karnaushenko,*[e] Volker Neu*[a], and Oliver G. Schmidt*[b,e,f]

[a]*Institute for Integrative Nanosciences, Leibniz IFW Dresden, 01069 Dresden, Germany.*
[b]*Nanophysics, Faculty of Physics, TU Dresden, 01062 Dresden, Germany.*
[c]*Departamento de Física, Universidad Católica del Norte, Avenida Angamos 0610, Casilla 1280, Antofagasta, Chile.*
[d]*Institute for Materials Science, TU Dresden, 01062 Dresden, Germany.*
[e]*Center for Materials, Architectures and Integration of Nanomembranes (MAIN), Chemnitz University of Technology, 09126 Chemnitz, Germany.*
[f]*Material Systems for Nanoelectronics, Chemnitz University of Technology, 09107 Chemnitz, Germany.*

E-mail: daniil.karnaushenko@main.tu-chemnitz.de
E-mail: V.Neu@ifw-dresden.de
Email: oliver.schmidt@main.tu-chemnitz.de

The PDF file includes:
Supplementary Figures S1 – S9;
Supplementary Notes 1 – 9.

Supplementary Figures

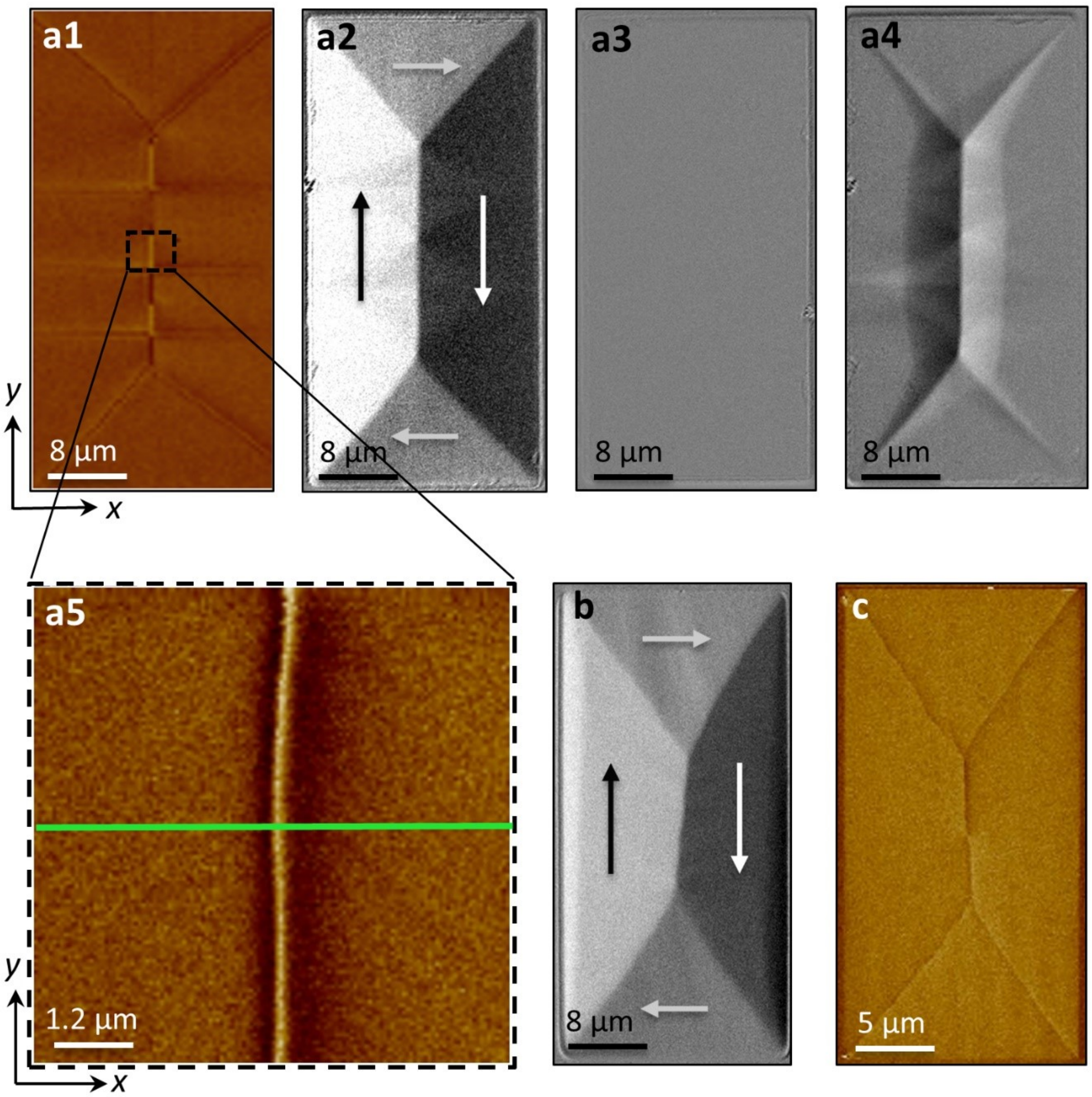

Fig. S1 Magnetic domain and domain wall configurations of three different Permalloy rectangles. (a) Rectangle 1, L = 50 µm, W = 25 µm, d = 50 nm. AC-demagnetized state imaged in (a1) magnetic force microscopy and (a2) Kerr microscopy. (a3) after background (Fig. S1a2) subtraction. (a4) Background subtracted image in the presence of ac-field along the rectangle's long axis. (a5) Magnified view of the area shown in the dashed square in Fig. S1(a1). The solid green line points to the line, where with the 'slow scan axis' disabled, low frequency (f = 0.01 Hz) domain wall oscillations are imaged. (b) Kerr image of ac-demagnetized state of rectangle 2, L = 50 µm, W = 25 µm, d = 20 nm. (c) MFM image of ac-demagnetized state of rectangle 3, L = 30 µm, W = 15 µm, d = 20 nm. The black and white arrows in the domains indicate the magnetization direction.

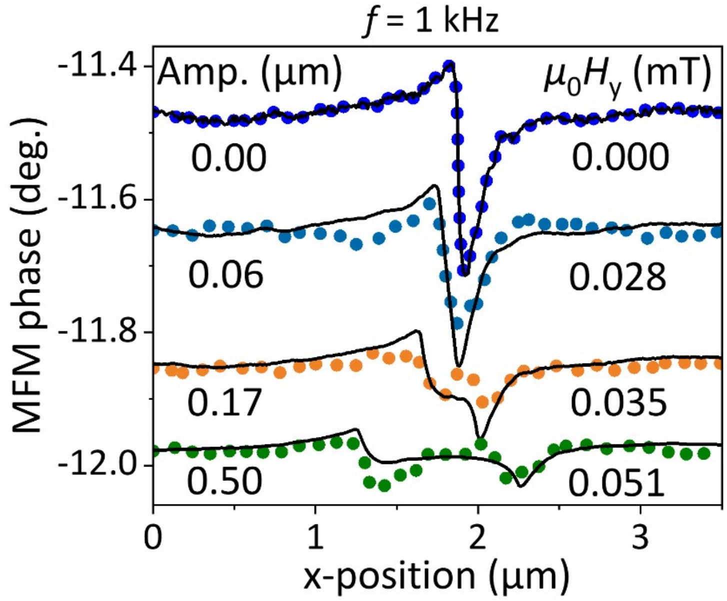

Fig. S2 Measured (colored dotted lines) and calculated (black solid lines) time-averaged MFM profiles for domain wall oscillations at different field amplitudes (at a constant frequency of 1 kHz) in rectangle 3 (L = 30 µm, W = 15 µm, d = 20 nm). $\mu_0 H_y$ represents the field strength, at which oscillation signals are recorded. Amp. (µm) represents the amplitude of sinusoidal oscillation, used to fit (solid black lines) the measured signal.

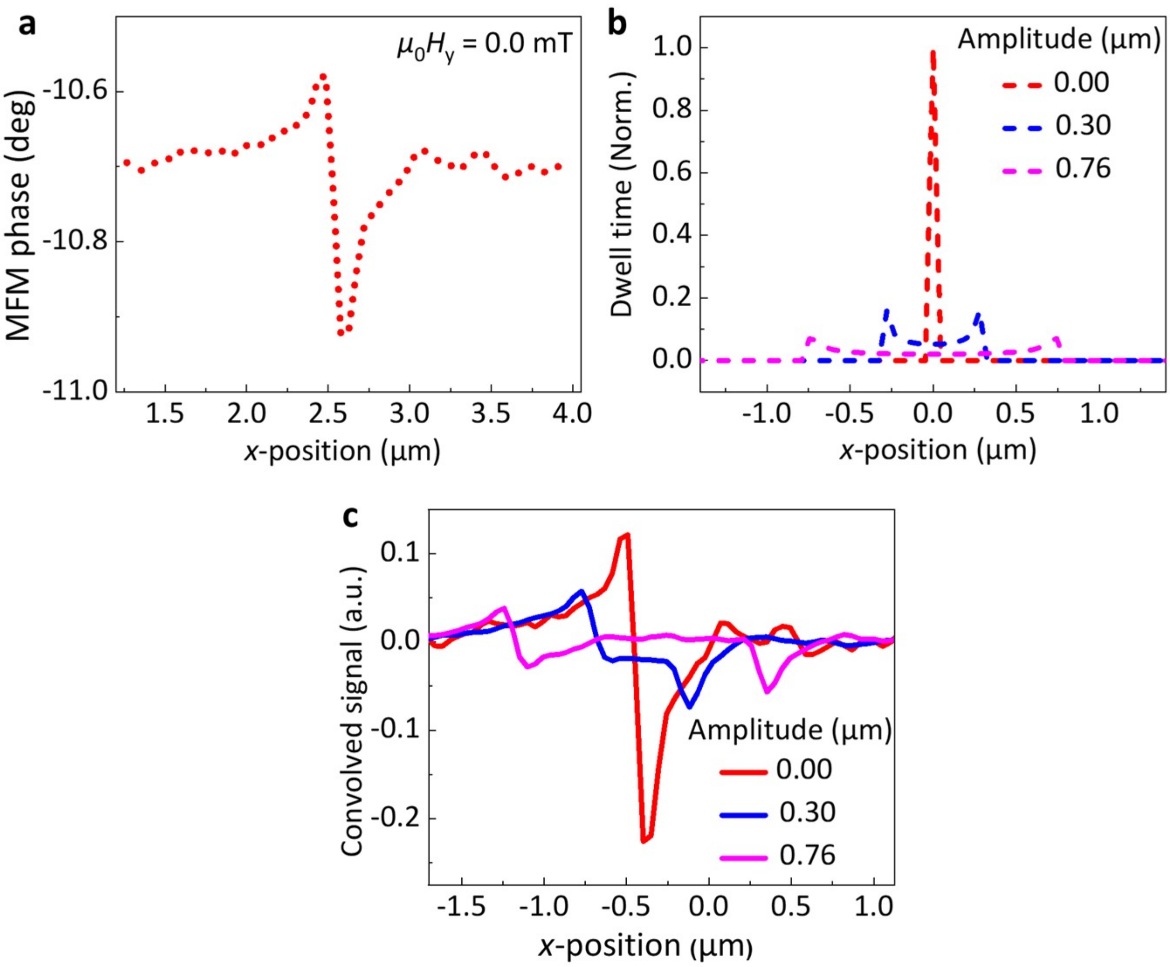

Fig. S3 Mathematical model for the time-averaged MFM imaging of domain wall oscillations. (a) Measured static domain wall profile (also shown in Fig. 2c, 2f). (b) Dwell time calculated for sinusoidally oscillating DW with different peak amplitudes (the 3D view is shown in Fig. 1b). (c) Calculated time-averaged MFM signal obtained after convolution of Dwell time profiles (b) with the static DW profile (a).

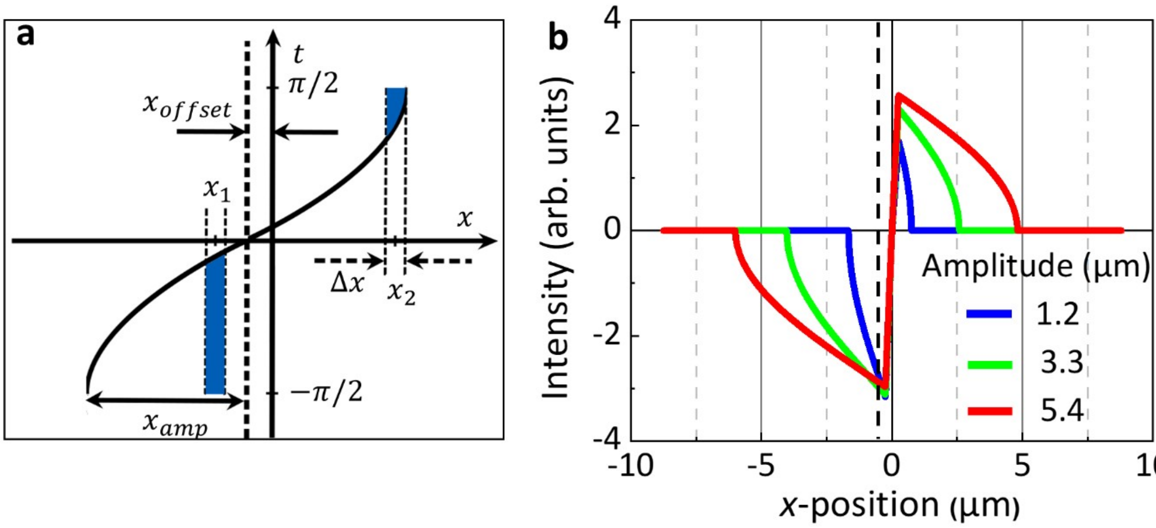

Fig. S4 Mathematical model for the time-averaged Kerr imaging of domain wall oscillations. (a) Schematic diagram showing average time (blue area) spent by the growing domain (due to sinusoidal oscillations of DW) at a given *x*-position (x_1, x_2) with sinusoidal oscillation being asymmetric (by x_{offset}) in the *x*-axis. (b) Calculated average time spent by domain at every *x*-position, values of amplitude shown in micro-meters are the ones used for fitting the experimental data shown in Fig. 3c.

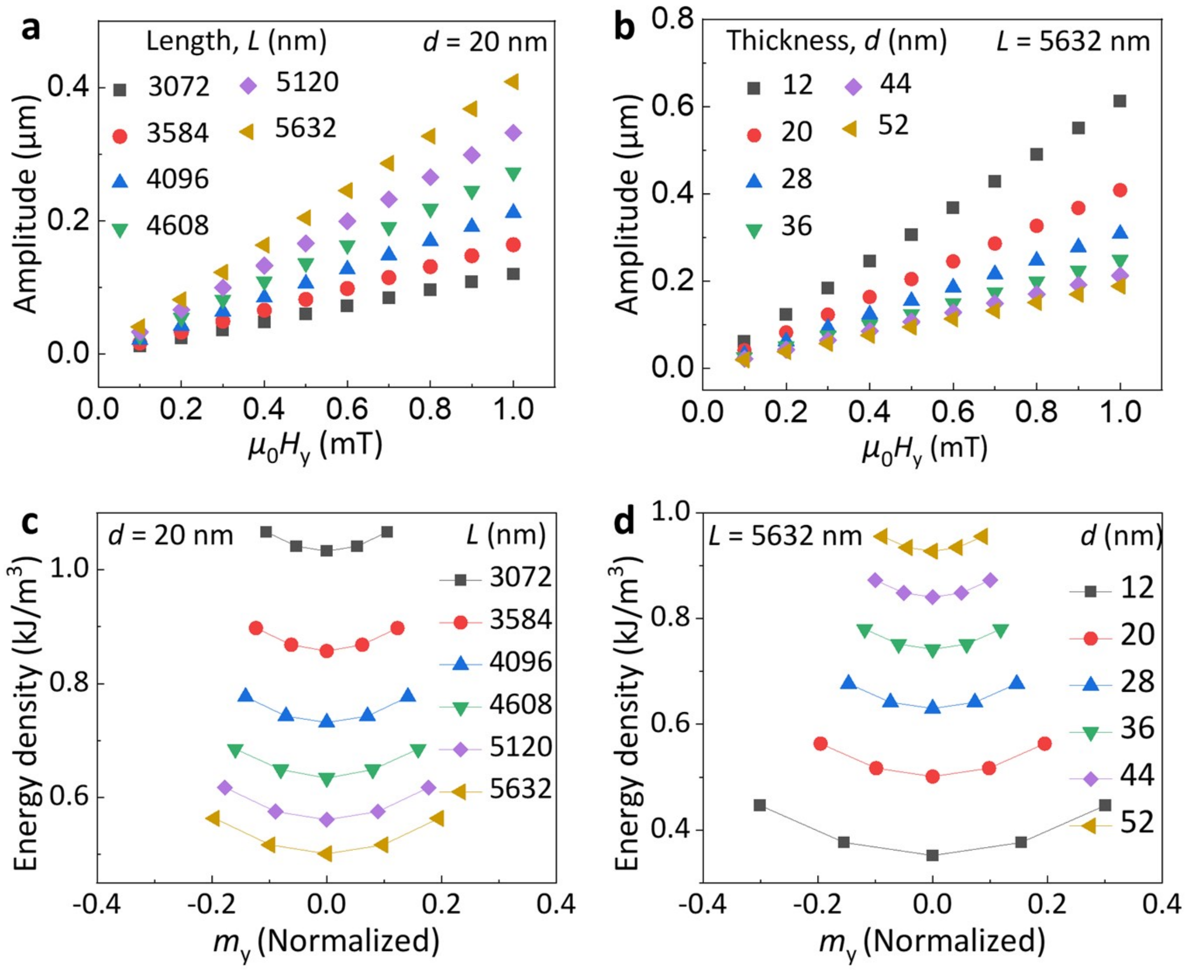

Fig. S5 Influence of structure size and thickness on the quasi-static DW dynamics obtained by micromagnetic OOMMF simulations. (a) dc-field induced DW oscillation amplitude as a function of applied magnetic field strength for different sizes of rectangles (varying length L while keeping the length to width aspect ratio *L*/*W* = 2:1 and thickness = 20 nm constant), (b) dc-field induced DW oscillation amplitude as a function of applied magnetic field strength for varying film thickness (for fixed length *L* = 5632 nm). (c) Energy density (demagnetizing + exchange) as a function of m_y (m_y is the normalized magnetization value for varying length *L*, (d) Energy density (demagnetizing + exchange) as a function of m_y for varying thickness *d*. Energy density *vs.* m_y plots has been used for extracting the stiffness parameter *c*, which is plotted in Fig. 5c and 5d.

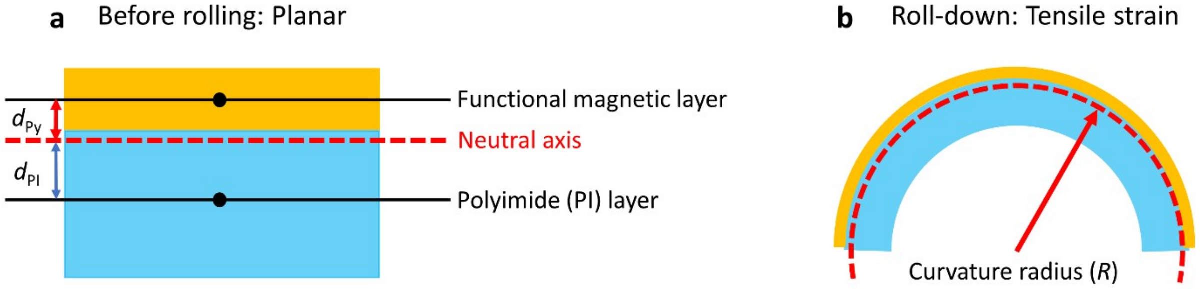

Fig. S6 Schematic illustration of the neutral axis and the cross-section of the functional magnetic layer deposited on top of the Polyimide film, (a) before rolling, (b) after rolling down.

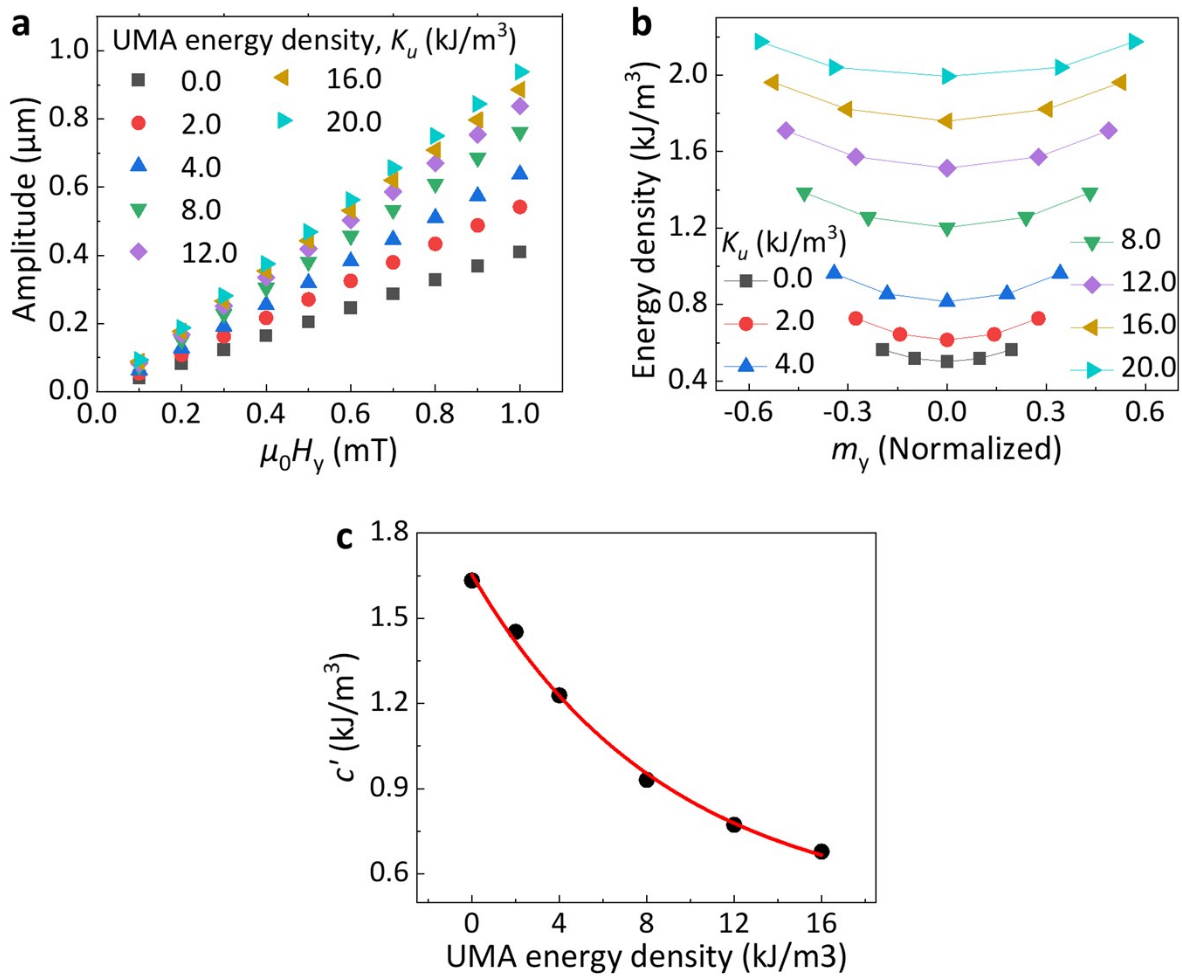

Fig. S7 Influence of induced uniaxial magnetic anisotropy (UMA) along rectangle's long axis on the quasi-static DW dynamics obtained by micromagnetic OOMMF simulations for a Py rectangle with L = 5632 nm, W = 2816 nm, and d = 20 nm. (a) DW oscillation amplitude as a function of applied magnetic field strength, (b) energy density (demagnetizing + exchange + UMA) as a function of m_y. Parabolic behavior has been fitted according to Eq. S10, (Supplementary Note 7) for extracting the stiffness parameter c'. (c) Stiffness parameter c' as a function of UMA energy density along long axis.

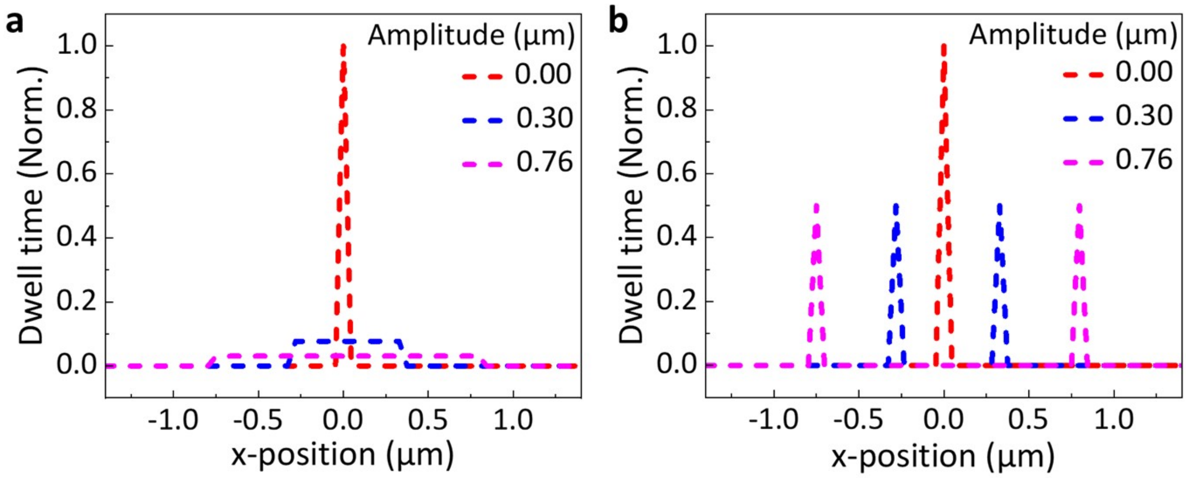

Fig. S8 Dwell-time function for (a) triangular and (b) square waveform.

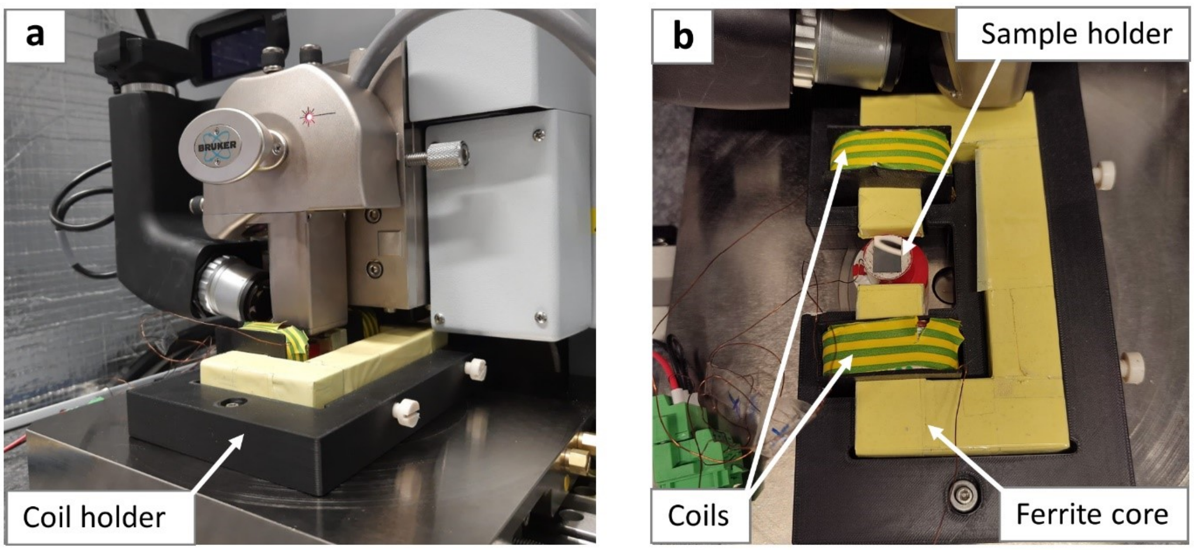

Fig. S9 MFM setup with electromagnetic coil. (a) MFM setup with the installed homemade coil, capable of generating in-plane dc- and ac-fields. (b) Magnefied view of MFM set up focused on coil.

Supplementary Notes

Supplementary Note 1. Static Domain and domain wall configuration in rectangles

Fig. S1(a1), S1(a2) and S1(a4) are the same images as shown in Fig. 2a, Fig. 3a and Fig. 3b, respectively. Additional weak contrast in MFM and Kerr images of 50 nm thick rectangle (Fig. S1a1, S1a2) is known as cross-tie walls, which are common in magnetic films with thicknesses between 30 nm and 90 nm[45]. Aiming to study field excited DW oscillations, a zero-field image, containing four domain state (Fig. S1a2) was used as a reference and subtracted from the live image before application of any external fields, thus, the difference image Fig. S1a3 displays no contrast. An external ac-field applied along the long axis of the rectangle drives the DW in phase with the applied excitation field and the DW dynamic region appears as a dark and bright contrast seen in Fig. S1a4.

Real-time imaging of a DW oscillating with 0.01 Hz (as shown in Fig. 2a) was performed with the slow scan axis disabled at the center of the Fig. S1a5 (shown in solid green line).

Kerr image Fig. S1b and MFM image S1c show the rectangle 2 and 3, respectively. For these structures of thickness 20 nm, cross-tie walls are absent.

Supplementary Note 2. Time-Averaged MFM imaging of DW oscillation in rectangle 3

For DW oscillation up to an amplitude of around 100 nm, the peak does not split, but becomes broader compared to the signal in the static regime, and only on increasing the field amplitude it splits into two minima as explained in the manuscript and shown in Fig. S2. Smallest peak oscillation amplitude is retrieved by the fitting procedure down to 60 nm. The visible deviation of the fitting functions from the measured MFM signal indicates a deviation of the DW oscillation from an ideal sinusoidal wall oscillation in rectangle 3 (L = 30 µm, W = 15 µm, d = 20 nm).

Possible reasons could be an asymmetric DW oscillation due to inhomogeneities in the pinning landscape. Or, slight changes in MFM tip's magnetic properties between scanning static and dynamic measurements.

Supplementary Note 3. Modeling of time-Averaged MFM signal (for DW oscillations in rectangle 1) with Dwell time function and static DW signal

Data acquired from the MFM image of the static DW (line profile is shown in Fig. S3a) is used to create oscillating DW signal, DW motion is assumed to follow a pure sin function $x_{DW}(t)$ = sin(t), as sketched in Fig. 2e of the main text.

Number of scan lines in static DW = n = 128.

Scan size of the static DW image = $x_{scan-size}$ = 5.95313 µm.

Resolution of image (size of one pixel) = $x_{res} = x_{i+1} - x_i$ (= $x_{scan-size}/(n-1)$ = 5.95313 µm/ (128 – 1)) = 0.046875 µm.

Calculation of the dwell time function for oscillating domain wall includes peak amplitude of DW oscillations (x_{amp}), resolution of MFM image ($x_{res} = x_{i+1} - x_i$) and scan size of MFM image.

Dwell time function:

Using above parameters (x_{amp} and x_{res}), the following discrete function calculates the dwell time at every x_i position with resolution x_{res} (Fig. 2e)

$$Dwell\ time,\ t_D(x_i) = \frac{1}{N}\left[\sin^{-1}\left\{\left(x_i + \frac{x_{res}}{2}\right)\Big/ x_{amp}\right\} - \sin^{-1}\left\{\left(x_i - \frac{x_{res}}{2}\right)\Big/ x_{amp}\right\}\right] \quad \text{(S1)}$$

Where N is the normalization factor

$$N = \sum_{i=-x_{scan-size}}^{x_{scan-size}}\left[\sin^{-1}\left\{\left(x_i + \frac{x_{res}}{2}\right)\Big/ x_{amp}\right\} - \sin^{-1}\left\{\left(x_i - \frac{x_{res}}{2}\right)\Big/ x_{amp}\right\}\right] \quad \text{(S2)}$$

Here, i runs from $-x_{scan-size}$ to $+x_{scan-size}$ with step of x_{res}, generating total of $2n-1$ (255) number of dwell time points, which is a requirement to fulfill convolution criteria.

The dwell time data is plotted in Fig. S3b for two different oscillation peak amplitudes (0.30 µm and 0.76 µm) including the one with 0.00 µm (delta peak) to mimic dwell time for static DW.

The convolution (Eq. S1) with the static DW profile (Fig. S3a, 128 points) generates the expected time-averaged MFM profile (128 points plotted in Fig. S3c) and is used to fit the experimentally measured time-averaged DW oscillations (1 kHz excitation frequency).

$$MFM_{ac}(x') = \sum_{x=-x_{scan-size}}^{x_{scan-size}} MFM_{static}(x)\, DT(x^{'}-x) \qquad (S3)$$

An important experimental condition is that all measurement parameters during dynamic DW imaging, such as MFM tip's magnetic properties and scanning parameter (scan rate, number of pixels per scan line, lift height) should be identical as they were during static DW imaging.

Additional information about MFM tip used for dynamics measurements: We consider any field-induced changes in the magnetization of the MFM tip negligible, as the maximum field applied to drive the DW is at least 100 times smaller than the typical switching field (40 - 95 mT) of the MFM tip.

Likewise, the influence of the used low moment (3.75 × 10-14 emu) MFM tip on the dynamics of the DW (reported measurements) is insignificant. The MFM tip did not act as an additional pinning potential for the moving DW, and the moving tip did not drag the DW. This can be seen in Fig. 2b, where the DW very smoothly follows the excitation field profile.

Furthermore, low moment tips are typically based on a thinner magnetic coating. Their choice is thus beneficial for achieving sharper features of the static DW and is therefore recommended for dynamics measurements to resolve oscillation amplitude of 100 nm or below.

Supplementary Note 4. Modeling of time-averaged Kerr signal

The following mathematical model for time-averaged Kerr imaging is an extension of the model presented in the main manuscript (description of Fig. 3). In addition to the oscillation amplitude (x_{amp}) and the resolution of the Kerr image ($x_{res} = \Delta x$) it includes a possible lateral offset in DW oscillation (x_{offset}) to fit the observed dynamic Kerr signal as shown in Fig. S4. With this we obtain the Dynamic Kerr intensity:

Dynamic Kerr intensity (x) = $$C.\int_a^b [(\pi/2)\cdot sign(x) - Sin^{-1}((x - x_{offset})/x_{amp})]dx \qquad \text{(S4)}$$

Where sign(x) is the sign function, C a scaling factor, x_{amp} the peak amplitude of DW oscillation and x_{offset} a lateral offset in the DW oscillation. The scaling actor C and x_{amp} are manually adjusted to match the Kerr intensity shown in Fig. 3c. The integration limits depend on the DW position x and are defined as

$a = max(x - \Delta x/2, -x_{amp})$; $b = min(x + \Delta x/2, x_{amp})$

An asymmetry in the bright and dark contrast is clear from the dotted line profiles shown in Fig. 3c and can be described by a x_{offset} = 0.5 µm, constant with increase in amplitude, using the above fitting function. One of the possible reasons for this asymmetry could be that the 180° DW in the initial zero-field state was not sitting exactly in the center of the structure.

Ideally, if the resolution of the Kerr image were infinitely large, the contrast change in the dynamic difference image at x = 0 should occur abruptly (with infinite slope). Due to the finite resolution, a resolution term (Δx or x_{res}) of around 115 nm (using 100x objective) was included to correctly model the finite slope across the contrast inversion.

Supplementary Note 5. Equilibrium position of 180° DW in Landau pattern in the presence of external magnetic field

The equilibrium DW position x_{amp} can be derived from the minimum of the total energy density

$$\varepsilon_{tot} = \varepsilon_{ex} + \varepsilon_{demag} + \varepsilon_{Zeeman} \tag{S5}$$

with respect to m_y via

$$\frac{\partial \varepsilon_{tot}}{\partial m_y} = 0, \tag{S6}$$

applying

$$\varepsilon_{Zeeman} = -\mu_0 \cdot M_s \cdot H \cdot m_y \tag{S7}$$

and

$$m_y = \beta \cdot \frac{2 \cdot x_{amp}}{W} = \beta \cdot \frac{4 \cdot x_{amp}}{L} \tag{S8}$$

Eq. S8 relies on a rigid 180° DW of constant length which is valid for moderate amplitudes. The factor β corrects for the closure domains with transverse magnetization. After substituting Eq. 4 from the main text and Eq. S5, S7 and S8 into Eq. S6, one derives

$$x_{amp} = \frac{\mu_0 M_s}{8\beta} . \frac{L}{c} . H \tag{S9}$$

Supplementary Note 6. Strain estimation of rolled geometries

This paragraph derives an estimate for the tensile strain experienced by the Py structure in the rolled down state (Fig. 6b2 in main text). Fig. S6a,b illustrates the cross-section of the layered structure consisting of magnetic layer and the Polyimide film together with the neutral axis for the bilayer structure. The neutral axis separates the region of compressive and tensile strain and is thus defied as a line of zero strain within the cross-section of the bilayer. The distances d_{PI} and d_{Py} in Fig. S6a denote the distances from the layer center of Polyimide and Permalloy film to the neutral axis. The thickness of Polyimide film and Permalloy films are 1200 nm and 100 nm, respectively, therefore,

$d_{PI} + d_{Py} = 650$ nm

Equilibrium requires,

$Y_{PI}.d_{PI}.A_{PI} - Y_{Py}.d_{Py}.A_{Py} = 0$

Where Y_{PI} (Y_{Py}) and A_{PI} (A_{Py}) are the Young's modulus and cross-sectional area of the Polyimide (Permalloy) film.

With the values $Y_{PI} = 3.2$ GPa and $Y_{Py} = 96.4$ GPa and above Eq., we obtain

$d_{Py} = 185$ nm.

Consequently, the center of the Permalloy film sits 185 nm above the neutral axis, which corresponds to an overall tensile strain in rolled-down state (Fig. S6b). The bending strain can be calculated via $\varepsilon = d_{Py}/R$, where R is the radius of the tube. With the experimentally observed bending radius 60 µm this results in 0.30 % tensile strain in the rolled-down Py structure. With the Youngs modulus of Py, $Y_{Py} = 96$ GPa, this corresponds to a positive stress in the rolling direction (perpendicular to the structure's long edge) of $\sigma \approx 288$ MPa = 288 MJ/m^3.

Supplementary Note 7. Influence of magnetic anisotropy: micromagnetic simulations

The following study is similar to the one discussed in details in Supplementary Note 5 but with an additional energy density, a uniaxial magnetic anisotropy (UMA), to explain the increase in DW oscillation amplitude for a rectangle in the strained state (as shown in Fig. S7a and Fig. 6c).

In rectangles with UMA, the equilibrium position in a given field is determined by the gain in Zeeman energy versus the costs of an increased exchange, demagnetization and anisotropy energy. For that, the sum of demagnetizing energy, exchange energy and uniaxial anisotropy energy was analyzed from the micromagnetic simulations as a function of m_y for small external fields around zero field (Fig. S7b). In all simulations, a quadratic increase in energy density with m_{y} was observed, which can be expressed as

$$\varepsilon_{ex + demag + UMA} = c_0 + c' \cdot m_y^2, \tag{S10}$$

where the stiffness parameter c' quantifies the restoring force on the DW when displaced from the equilibrium position $m_{\mathrm{y}} = 0$. This parameter for the rectangle as a function of UMA energy density (K_u) is given in the Fig. S7c, and shows an exponential decay which can be described as $c' \propto exp\left(\frac{-K_u}{9}\right)$.

The equilibrium DW position x_{amp} can now be derived from the minimum of the total energy density $\varepsilon_{tot} = \varepsilon_{ex} + \varepsilon_{demag} + \varepsilon_{Zeeman} + \varepsilon_{UMA}$ (S11)

Parameter β used in Eq. S8 is constant, as the ratio of closure domains (domains aligned with short axis of rectangle) to basic domains remains constant on increasing length or thickness of rectangles. Contrary, this ratio decreases (due to an increase in 180° wall length) on increasing the UMA magnitude along long axis. This reduced ratio is clearly visible in Fig. 6c-iii where the closure domains size is reduced after bending the rectangle. Therefore, we replace parameter β by β' (which is a function of UMA) in Eq. S8 and substituting Eqs. S10, S11 and S8 into Eq. (S6), one derives at

$$x_{amp} = \frac{\mu_0 M_s}{8\beta'} . \frac{L}{c'} . H \tag{S12}$$

Eq. (S12) with c' and variable β' is used to fit the x_{amp} *vs.* UMA energy density plot (Fig. 6d).

Supplementary Note 8. Modeling of time-Averaged MFM signal for non-sinusoidal DW oscillations

While the experimentally observed DW motion is expected to largely follow the sinusoidal field excitation, deviations from a pure sinusoidal DW motion will nevertheless be detectable in the time-averaged MFM signal, as long as the periodicity of the motion is not violated. This is illustrated for two extreme cases of a triangular and a rectangular waveform in Fig. S8. The calculation of the dwell time function $t_D(x)$ follows the exact same equations as outlined in Supplementary Note 3, equations S1 and S2, except that $\sin^{-1}$(argument) is replaced by the inverse of the now assumed periodic function (triangular or square). The dwell time function clearly differs from that of a sinusoidal DW motion, and again bears a clear signature of the oscillation amplitude (Fig. S8). In case of the triangular waveform, the constant DW velocity leads to a constant dwell time within the limits of the motion (i.e. the return points defining the oscillation amplitude), while the rectangular waveform leads to largely enhanced dwell time peaks at the return points, where the DW rests before it abruptly jumps to the opposite return point.

Supplementary Note 9. Electromagnetic coils to apply in-plane field during MFM measurements

Fig. S9a illustrates the MFM setup with electromagnetic coils mounted on the MFM stage with the help of a holder that can be fixed to the MFM stage. The setup is capable of applying in-plane dc- and ac-fields to the sample placed on the sample holder. Two electromagnetic coils (750 windings, 20 mH) were manufactured using 3D printed frames and enameled copper wires. The home build ferrite core was inserted inside the coils and placed with the sample holder as shown in Fig. S9b. Ferrite core with square cross-section (15 mm × 15 mm) was manufactured by cutting thin ferrite sheets (120 mm × 120 mm × 0.3 mm) into the shape as shown in Fig. S9b and stacking them to the desired thickness. The high permeability value of 200 – 250 (up to MHz frequency) of ferrite core allows to generate ac-fields of up to 0.25 mT at 1 kHz frequency.